AuPd-nNiO as an effective catalyst for the base-free oxidation of HMF under mild reaction conditions

ARTICLE

AuPd-nNiO as effective catalyst for the base -free oxidation of HMF at mild reaction conditions

Received 00th January 20xx,
Accepted 00th January 20xx

DOI: 10.1039/x0xx00000x

Danilo Bonincontro,[a] Alice Lolli,[a] Alberto Villa,*[b] Laura Prati,[b] Nikolaos Dimitratos,[a] Gabriel M. Veith,[c] Lidia E. Chinchilla,[d] Gianlugi A. Botton,[d] Fabrizio Cavani,[a] Stefania Albonetti *[a]

Au-based catalysts supported on nanosized NiO (nNiO) were synthesized and were investigated in the oxidation of 5-hydroxymethylfurfural (HMF) to 2,5-furandicarboxylic acid (FDCA) in base-free conditions using molecular oxygen as the oxidant, at 90°C. By choosing the optimal composition of Au-Pd nanoparticles (6:4 Au/Pd atomic ratio), we report an efficient and stable nNiO-supported Au-Pd alloy catalyst. The presence of nNiO and Au-Pd nanoparticles on the surface was essential to achieve high conversion (95%) and high activity, high yield to FDCA (70%) and good level of stability. Significant synergistic effects were observed between Au and Pd in the alloy as well as on NiO. The present work provides mechanistic insights to the alloying effect and support-metal interaction in terms of understanding better the role of alloy and support in affecting specific reaction pathways. Finally, the outcome of this knowledge can help developing efficient catalysts for the aerobic oxidation of biomass-derived molecules under base-free conditions in water and mild reaction conditions.

Introduction

The need to decrease the dependence on fossil feedstocks to produce fuels, chemicals and materials, has led scientists to look for sustainable alternatives. In this context, non-edible lignocellulosic biomass , have been pointed out as suitable renewable resources in the replacement of non-renewable raw materials for the synthesis of useful chemicals thanks to their abundance and availability.[1] To achieve this goal, different approaches have been suggested. Among them, one of the most investigated relies on the conversion of the renewable raw material into the so called "platform molecules", i.e. versatile intermediates which can be converted, on their turn, into different high added value chemicals.[2] 5-(hydroxymethyl)furfural (HMF), a platform chemical obtained by fructose dehydration,[3] could be considered as one of the most representative examples, since it could be converted through different chemical approaches into several chemicals. The applications of synthesised chemicals are mainly related to polymer industry,[4] such as furandicarboxylic acid (FDCA). Indeed, the latter has been proven to be a suitable monomer for the synthesis of polyesters, such as polyethylene furanoate (PEF), a potential polymer to be used in soft drinks bottling,[5, 6] as replacement of the oil-derived PET, with an annual estimated production of 25 million tons in 2018.[7] The HMF conversion into FDCA has been investigated using a number of catalytic, electrocatalytic and biocatalytic processes[8] and typically occurs via consecutive oxidation of the two moieties bonded to the furan ring leading to a stepwise pathway, as reported in Scheme 1. One of the most relevant industrial attempt to obtain FDCA by HMF oxidation relies on the catalysts and technologies developed in the AMOCO process for the oxidation of paraxylene to terephthalic acid.[9] In these operative conditions, HMF is converted through the route "a" illustrated in Scheme 1.[10] However, the use of homogeneous catalyst (Co and Mn acetate) and corrosive solvent (acetic acid) can be considered as the main shortcomings of this process. Thus, efforts have been devoted to the design of heterogeneous catalysts,[11] and, in this frame, the effectiveness of supported metal (mainly Au, Pd, Pt) nanoparticles (NPs) in aqueous phase conditions has been disclosed. As far as the use of supported Au NPs is concerned, it has been found that high yield of FDCA can be obtained in mild temperature (50-90°C) under strongly basic conditions (pH=9-13), obtained by addition of inorganic soluble bases (typically, NaOH and Na_2CO_3).[12-16] In such high pH condition, it has been proven that the reaction pathway involved differs from the previously described one, since HMF conversion into FDCA passes through HMFCA as intermediate (route b Scheme 1), being the formation of the latter strongly favored respect to DFF (route Scheme 1) under basic conditions.[17]

Further studies demonstrated that, gold based catalyst's activity could be improved by preparing alloyed bimetallic nanoparticles, such as reported for Au/Cu-TiO_2 (with a Au:Cu ratio equal to 3:1)[18] and Au/Pd-TiO_2 (with a Au:Pd ratio equal to 6:1).[19] This feature has been ascribed to the modification of the electronic

[a] Department of Industrial Chemistry "Toso Montanari", University of Bologna, Viale Risorgimento 4, 40136 Bologna, Italy. E-Mail: Stefania.albonetti@unibo.it
[b] Department of Chemistry, University of Milan, Via Golgi 19, 20133 Milan, Italy. E-Mail: Alberto.villa@unimi.it
[c] Chemical Science Division, Oak Ridge Laboratory, Oak Ridge, TN 37831, USA
[d] Canadian Centre of Electron Microscopy and Department of Material Science and Engineering, McMaster University, 1280 Main Street West, Hamilton, Ontario L8S 4M1, Canada

† Footnotes relating to the title and/or authors should appear here.
Electronic Supplementary Information (ESI) available: [Fig S1-S7: STEM-HAADF images XPS spectra of the catalysts; Table S1 Comparison with the literature; Table S1-S2 additional catalytic data. See DOI: 10.1039/x0xx00000x

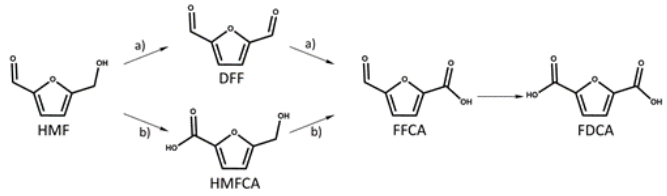

Scheme 1 HMF to FDCA possible routes

properties of the original metal (i.e. gold) which arises from the preparation of the alloyed systems, that, on its turn, leads to a cooperative effect that enhances the catalytic properties of the monometallic system. However, even if lower amount of base were used with some bimetallic catalysts, the presence of NaOH is still the main concern from the industrial point of view.

In fact, the main drawback related to the use of the abovementioned gold-based catalysts is linked to the necessity of working at very high pH, lowering the overall mass efficiency of the reaction, since large excess of inorganic bases (from 2 to 20 equivalents respect to the HMF) are required to reach good FDCA yield. Thus, the latest trend in HMF oxidation has been focusing the development of catalytic systems able to perform HMF oxidation under base-free conditions. In this frame, it has been proven that by choosing suitable supports for metallic nanoparticles it is possible to bypass the addition of the base to the reaction mixture. For instance, carbon based material were found to be suitable supports: functionalised carbon nanotubes (CNT) were used as support for both alloyed Au/Pd[20] and monometallic Pt NPs,[21] leading to highly active systems (FDCA yield 94 and 98%, respectively). In these reports no HMFCA was detected in the reaction mixture indicating that, under base-free conditions, the reaction pathway involves DFF as intermediate (route "a", Scheme 1). Alternatively, a different approach is based on the use of intrinsically basic supports, such as hydrotalcite (HT)[22] or solid layered hydroxide.[23] In these cases the reaction pathway seems to involve HMFCA production (route "b" Scheme 1) even though no homogeneous bases were added to the reaction mixture. In addition, it must be noted that, in absence of homogenous base, higher temperatures are usually required to perform the oxidation than the ones required to carry out the reaction under basic conditions. Palkovits and co-workers reported Ruthenium catalysts supported on covalent triazine frameworks (CTF) to be active and selective under base-free conditions for HMF oxidation using air as the chosen oxidant with high conversion (99.9%) and yield (36.6%), at 140 °C and 20 bar of synthetic air and good recyclability. The authors claim the improved activity and stability of Ru/CTF based on the formation of mesoporous CTFs materials and the high degree of polarity.[24] In another study, the usage of commercial Ru/C catalyst was reported as an efficient catalytic system for the base-free conversion of HMF to FDCA and low degree of deactivation.[25] The authors reported that the favoured oxidation reaction pathway is following the DFF/FFCA route rather than the HFCA pathway. Recently, a new class of $MnCo_2O_4$ spinel supported Ru catalysts were reported to be active and selective under base-free conditions.[26] The authors attributed the high activity observed based on the availability of both Lewis and Brønsted acid sites on the surface of the $Ru/MnCo_2O_4$ catalyst, which was confirmed by NH_3-TPD characterization studies and the presence of Ru metallic species with small particle size. Moreover, another green alternative catalytic system was reported by S. Zhang and co-workers,[27] combining non-noble metal catalysts containing Ce, Fe, Zr and the usage of ionic liquids for promoting the base-free conversion of HMF. $Ce_{0.5}Fe_{0.15}Zr_{0.35}O_2$ catalyst was reported to have high conversion (99.9% conversion) and moderate yield to FDCA (44.2%) at 160 °C after 24 h of reaction, due to the existence of active iron and zirconium species and the formation of CeO_2-based solid solution that could facilitate the formation of oxygen vacancies and therefore to improve the redox properties of the catalyst.

Recently, Villa and co-workers demonstrated the possibility to oxidize benzyl alcohol and other well-known aromatic and aliphatic alcohols under base free conditions using metal nanoparticles supported on nickel oxide supports[28]. They demonstrated that the use of nanometric NiO (nNiO) greatly improved catalyst activity, mainly because of a cooperative effect between Au and NiO. Moreover, NiO can be used as a basic support for promoting HMF reaction.

Therefore, in the present study, Au, Pd and Au/Pd nanoparticles (Au:Pd metal molar ratio equal to 6:4, as a model well-defined bimetallic catalyst for the upgrade of a range of biomass and polyol-derived molecules[29]) were deposited on nNiO and their catalytic behaviour was evaluated in the liquid-phase oxidation of HMF in base-free conditions, demonstrating the possibility to obtain high yield FDCA without the addition of any inorganic base. This study highlights the importance of catalyst synthesis for the improvement of sustainable chemical processes.

Experimental

Catalyst preparation

nNiO has been prepared following the procedure reported elsewhere.[30] $Ni(NO_3)_2$ x $6H_2O$ (5 x 10^{-4} M) (Sigma-Aldrich, purity > 99.9%) and urea (Sigma-Aldrich, purity > 99.5%) (urea/Ni 10 : 1 mol mol^{-1}) were added to 200 ml of water under magnetic stirring. The solution was kept stirring for 6 h at 80 °C. The $Ni(OH)_2$ was separated from the solution by filtration and washed several times. The powder was dried at 60 °C for 12 h and then calcined at 300 °C for 3 h in static air.

Au-nNiO: Solid $NaAuCl_4 \bullet 2H_2O$ (0.051 mmol) and PVA (1%wt) solution (Au/PVA =1/0.5 wt/wt) were added to 100 mL of H_2O. After 5 min, a fresh solution of $NaBH_4$ (0.1 M) (Au/$NaBH_4$ 1/4 mol/mol) was added to the solution under stirring. Within a few minutes of sol generation, the colloid was immobilized by adding the support under vigorous stirring. The amount of support was calculated as having a total final nominal metal loading of 1 wt. %. After 2 h the slurry was filtered, the catalyst washed thoroughly with distilled water and dried at 80 °C for 4 h.

Pd-nNiO: Solid $Na_2PdCl_4 \bullet 2H_2O$ (0.051 mmol) and PVA (1%wt) solution (Pd/PVA =1/0.5 wt/wt) were added to 100 mL of H_2O. After 5 min, a fresh solution of $NaBH_4$ (0.1 M) (Pd/$NaBH_4$ 1/8 mol/mol) was added to the solution under stirring. Within a few minutes of sol generation, the colloid was immobilized by adding the support under vigorous stirring. The amount of support was calculated as having a total final nominal metal loading of 1 wt.

%. After 2 h the slurry was filtered, the catalyst washed thoroughly with distilled water and dried at 80 °C for 4 h.

AuPd-nNiO: Solid $NaAuCl_4 \bullet 2H_2O$ (0.031 mmol) and $Na_2PdCl_4 \bullet 2H_2O$ (0.020 mmol) (Au/Pd 6:4 mol/mol) and PVA (1%wt) solution (Pd/PVA =1/0.5 wt/wt) were added to 100 mL of H_2O. After 5 min, a fresh solution of $NaBH_4$ (0.1 M) (Pd/$NaBH_4$ 1/8 mol/mol) was added to the solution under stirring. Within a few minutes of sol generation, the colloid was immobilized by adding the support under vigorous stirring. The amount of support was calculated as having a total final nominal metal loading of 1 wt. %. After 2 h the slurry was filtered, the catalyst washed thoroughly with distilled water and dried at 80 °C for 4 h.

Catalyst characterisation

TEM: Samples for transmission electron microscopy (TEM) studies were prepared by depositing small amounts of dry catalyst powder onto holey carbon copper grids. Micrographs combined with analytical studies by energy-dispersive X-ray (XEDS) and electron energy loss spectroscopy were performed in High Annular Dark Field mode using a FEI Titan3 80-300 microscope operated at 80kV. Digital Micrograph, TIA, and INCA software's were used for the analysis of the TEM micrographs and XEDS spectra. The PSD, Gaussian fit, average particle diameter, and metal dispersion were calculated assuming a truncated cubooctaedron particle shape using Gauss software. EELS data including drift correction base on the zero-loss peak, background subtraction, and principal component analysis (PCA), were processed using Gatan's Digital Micrograph and Hyperspy software's.

X-ray photoelectron spectroscopy (XPS) data were collected using a PHI 3056 XPS with an Al anode source operated at 15kV and an applied power of 350W. The energy scale calibration of the instrument is checked using a sputter cleaned piece of Ag. Samples were manually pressed between two pieces of indium foil; the piece of In foil with the sample on it was then mounted to the sample holder with a piece of carbon tape (Nisshin E.M. Co. LTD). The lowest C1s BE species were shifted about 0.1 eV to 284.8 eV for comparison to literature values. There were no treatments (i.e. cleaning, heating, processing) to the samples before the XPS measurements. High resolution scans were acquired with a 23.5 eV pass energy and 0.05 eV steps a minimum of 50 times; survey scans were measured with a 93.9 eV pass energy and 0.5 eV energy steps a minimum of 25 times. Surface concentrations are calculated by integrating the peaks area and using standard atomic sensitivity factors supplied by the equipment manufacturer. The spectra were deconvoluted using Gaussian-Lorentzian functions and a Shirley-type background.

Catalytic tests

The catalytic tests were performed in a lab scale autoclave reactor (100 mL capacity from Parr), equipped with a mechanical stirrer (0–600 rpm) and sensors for measuring temperature and pressure. The aqueous solution of HMF (25mL, 0.02M) and catalyst (HMF/total metal molar ratio = 100) were loaded in the reactor. HMF (purity >99%) was purchased from AVABiochem and used without any purification.

The autoclave reactor was purged 3 times with O2 (2 bar) and then pressurized at 10 bar. The temperature was increased to the set point (90 °C) and the reaction mixture was stirred at 400 rpm for the whole duration of the experiment. Initial time (time zero) for the reaction was considered when the set point temperature was reached (after 10 min). At the end of the reaction, the reactor was cooled down to room temperature and the solution was filtered. Then, 1mL of the reaction mixture was collected and diluted 5 times and, the resulting solution was then analysed with an Agilent Infinity 1260 liquid chromatograph equipped with an Aminex HPX-87H 300 mm × 7.8 mm column (0.005 M H_2SO_4 solution as mobile phase) and a diode array detector. The compound quantifications were calculated from the peak areas after calibration using commercially available samples.

Recycling tests have been performed by reusing the recovered catalyst without any further cleaning procedure.

Results and discussion

Catalyst characterisation

The morphology of the prepared catalysts was analyzed by transmission electron microscopy (TEM). The as-prepared Au nanoparticles on nNiO had an average particle diameter of 5.2 nm (Table 1) with the presence of large aggregated nanoparticles (Figure S1). Smaller nanoparticles with an average diameter of 3.6 nm where obtained for Pd-nNiO as it is shown in Table 1. Moreover, similar to the previous case aggregates of Pd nanoparticles were observed (Figure S2). TEM analysis of AuPd-nNiO sample showed the presence of two different types of structures: small nanoparticles with an average particle size of 3.3 nm and accumulated particles forming aggregates (Figure S3). The EELS map (Figure 1) obtained from a typical nanoparticle confirms that both Au (red) and Pd (green) metallic components are intimately mixed within the nanostructure and clearly shows that the Pd virtually forms a thin layer around Au-Pd core particle. Furthermore, the (S)TEM-EDS analysis confirms that all metal nanoparticles analyzed are alloy structures (Figure 2). The obtained gold and palladium concentration reveals an atomic ratio close to 1.5Au:1Pd which is similar to the nominal value. However, the larger agglomerated structures were found slightly gold rich, being the atomic ratio close to 2Au:1Pd alloy structures.

Evaluation of Au4f data for Au-nNiO, revealed the presence of one specie with BE 83.9 eV, which can be attributed to the presence of metallic Au (Table 1).[31, 32] Evaluation of the Pd 3d data for Pd-NiO showed the presence of two Pd $3d_{5/2}$ species with binding energies of 335.6 and 337.4 eV attributed to Pd^0 and 23% oxidized $Pd^{\delta+}$ respectively (Table 1).[33] The oxidized Pd makes up a minority of Pd in the samples and is likely due to surface oxidation from the reaction with atmospheric O_2.[34]

Furthermore, this appears consistent with other reports of Pd catalysts supported on C and C-N type supports indicating no clear transfer of electron density to the nNiO.[35]

Table 1 Statistical median, standard deviation of the particle size and XPS for the Au-nNio, Pd-nNiO, and AuPd-nNiO catalysts.

Catalyst	Statistical median [nm]	Standard deviation (s)	Pd $3d_{5/2}$		Au $4f_{7/2}$	
			Pd^0	Pd^{2+}	Au^0	$Au^{\delta+}$
Au-nNiO	5.2	2.2	-	-	83.9 eV	-
					100%	
Au-nNiO used 15 min	6.3	2.5	-	-	84.1 eV	-
					100%	
Au-nNiO used 30 min	5.9	2.0	-	-	84.2 eV	-
					100%	
Au-nNiO used 6 h	6.1	2.2	-	-	84.0 eV	-
					100%	
Pd-nNiO fresh	3.6	0.8	335.6 eV	337.4 eV	-	-
			77%	23%		
AuPd-nNiO fresh	3.3	1.1	335.6 eV	337.5 eV	83.6 eV	84.9 eV
			76%	24%	90%	10%
AuPd-nNiO after 4 uses	3.6	1.4	335.2 eV	338.2 eV	84.1 eV	n.d.
			n.d.	n.d.	n.d.	n.d.

n.d.=not determined

The $Pd3d_{3/2}$ peaks were present at 341.0 and 343.4 eV due to Pd^0 and $Pd^{\delta+}$ respectively. After the addition of gold to the catalyst formulation the resulting $Au4f_{7/2}$ spectra has evidence for the presence of two Au species with binding energies of 83.6 eV and 84.9 eV as it is shown in Figure 3c. This is consistent with the formation of Au^0 and Au^+.[32] The presence of $Au^{\delta+}$ (10%) can be due to the incomplete reduction of gold. The slight negative shift in Au^0 binding energy from gold foil (84.0) is likely due to the interaction of Au-Pd due to the formation and presence of AuPd alloy nanoparticles and smaller particle size with respect to the monometallic Au sample.[36-38] This behavior has been already observed in the case of AuPt alloy.[39, 40] With the addition of gold there appears to be no change in the $Pd3d_{3/2}$ XPS data, Figure S4, lower left, indicating that the Pd remains mostly reduced with only about 24% of the Pd oxidized.

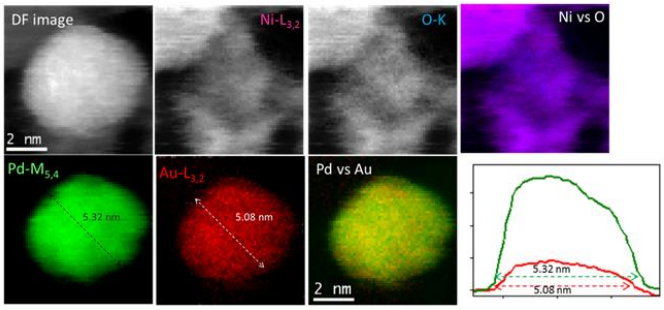

Figure 1 Elemental mapping of AuPd-nNiO using electron energy loss spectroscopy (EELS)

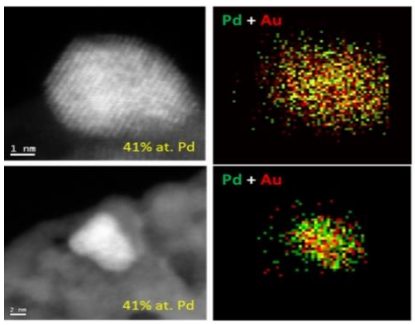

Figure 2 XEDS mapping of two representing AuPd particles.

In all the catalyst, the Ni 2p data shows the presence of two low energy peaks (854.0 and 856.0 eV) which are attributed to the presence of nNiO and $Ni(OH)_2$ species on the surface of the support (Figure S4). This assignment is supported by the O1s data which shows three peaks at 529.3, 531.0, and 532.9 eV due to Ni-O, Ni-OH and –OH species. There is very little residual carbon on the surface of the catalysts from adventitious carbon or residual PVA (< 0.3 at%) so the O1s spectra is not due to residual surfactant.

Catalyst screening

The activity toward HMF oxidation under base free condition of the prepared materials was evaluated (figure 3)

The results of this preliminary screening demonstrated the inability of the bare support to catalyse the reaction under base free conditions with conversion levels below 5%. Similarly, Pd-NiO sample did not show any relevant catalytic activity but the presence of small amount of DFF beside HMFCA at the end of the reaction, demonstrated the possibility to follow, in the reported conditions, both a and b reaction pathways reported in Scheme 1. The use of an increased reaction time (15h) led to very similar catalytic results; moreover, the introduction of NaOH (HMF/NaOH molar ratio 2) confirmed the inability of Pd-NiO to convert HMF also at high pH. Indeed, these conditions just promoted the formation of by-products due to HMF decomposition (77% HMF conversion was reached but 54% of carbon loss was observed, Table S2). On the contrary, the

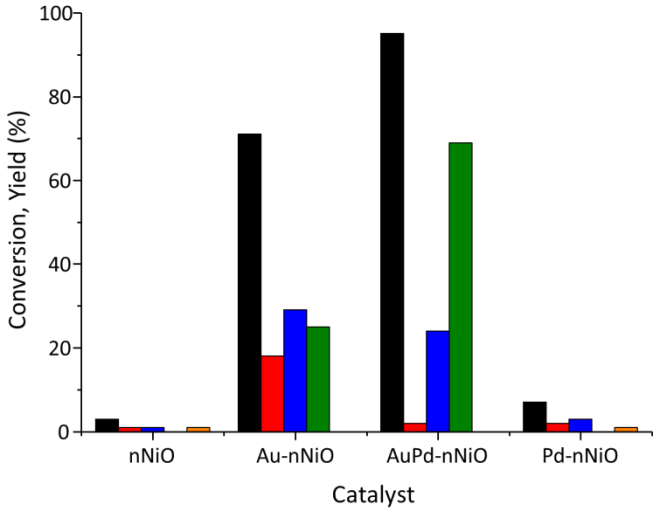

Figure 3 HMF conversion and product yields for the prepared Au, AuPd and Pd catalysts supported on nNiO. Reaction conditions: 90 °C, 6h, 10 bar O_2, HMF/total metal molar ratio = 100. Legend: ■ HMF conversion, ■ HMFCA yield, ■ FFCA yield, ■ FDCA yield, ■ DFF yield.

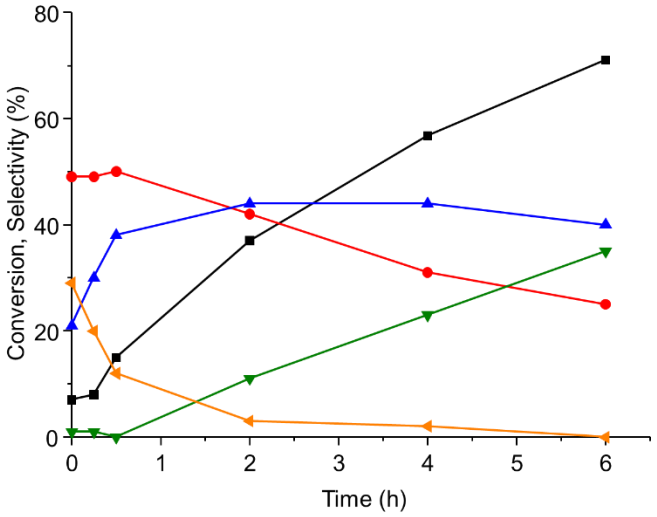

Figure 4 HMF Conversion and product selectivity as a function of time using Au-nNiO. Reaction conditions: 90 °C, 10 bar O_2, HMF/total metal molar ratio = 100. Legend: ■ HMF conversion, ● HMFCA selectivity, ◀ DFF selectivity, ▲ FFCA selectivity, ▶ FDCA selectivity.

results obtained using Au-nNiO sample clearly demonstrate that, even without the addition of base, 71% of HMF was converted after 6h of reaction. Both HMFCA and FFCA were formed at the end of the process and FDCA was produced with 25% of final yield. These promising results encouraged to investigate the synthesis of bimetallic supported nanoparticles using NiO as the desired support.

The preparation of a bimetallic Au/Pd system (Au:Pd molar ratio 6:4) led to a significant increase in terms of activity and especially of yield (95% of HMF conversion and 69% FDCA yield), confirming once again that the alloyed bimetallic structure enhances the catalytic performance of the parent metal, as already reported with titania[19] and active carbon supported materials (AC) with similar Au:Pd molar ratio.[41] However, it is noteworthy to emphasise that using nNiO as support the reactions are carried out under base-free conditions, indicating the important role of the support itself. Indeed, it is possible to hypothesize that the nNiO support changes the electronic and geometrical properties of the metal affecting the substrate binding on the metal/support interface and therefore HMF conversion is completed even without the presence of a base. The catalytic results obtained using Au-nNiO and AuPd-nNiO samples indicated the presence of high amount of FFCA intermediate after 6 h of reaction (25%). This result suggests that under base-free conditions the ratios of the reaction rates of the single steps involved in the HMF oxidation pathway is different respect to those reported for the same reaction conducted under basic conditions. In fact, at high pH, Au/Pd NPs containing catalysts, formed HMFCA as main intermediate while FFCA is quickly converted to FDCA, being the conversion of the HMFCA alcoholic moiety the rate limiting step of the reaction.[42] On the contrary, in the studied base-free HMF oxidation using nNiO supported systems, a significant change in the reaction rates seems to be present, with a strong drop in the transformation rate of FFCA to FDCA. Therefore, we focus our studies on the understanding of the catalytic and structural properties of the two gold-based (monometallic and bimetallic) systems.

Au-nNiO

HMF conversion and selectivity as a function of time for Au-nNiO catalyst is shown in Figure 4. The reported data show that Au-nNiO sample is able to convert HMF in base-free conditions even during the induction time, obtaining 7% of HMF conversion when the set point temperature (90 °C) is reached (t=0). In the early stages of the reaction, HMFCA and DFF were the main products detected, meaning that both reaction pathways showed in Scheme 1 can occur. However, the selectivities of these two intermediates evolved differently: DFF selectivity steadily dropped within the first 30 minutes, while HMFCA one was nearly steady within the same period, with a constant decrease starting from 30 minutes on. FFCA formation started at t=0 and its selectivity increased within the first 2h. Since at t=0 FFCA was already present in the reaction medium; it could be hypothesised that this intermediate derived from DFF conversion since HMFCA was not converted in the first 30 minutes of reaction. Moreover, the presence of a lower amount of DFF at t=0 compared to HMFCA, could be ascribed to a faster conversion of the former. FDCA formation started after 30 minutes, i.e. exactly when HMFCA was converted to FFCA, suggesting that FDCA production was probably achieved through reaction pathway which does not involve DFF formation.

Therefore, the reported data indicate that, using Au-nNiO sample, significant changes in product selectivities were observed after 30 minutes of reaction. Indeed, in the earliest reaction stage, HMFCA and DFF were produced in parallel pathways, with different reaction rates and can be both considered as primary intermediates of HMF oxidation. On the other hand, FFCA formation increased up to 40% in the early period of the reaction and then its selectivity remained constant with time, probably due to a similar rate of formation and

conversion to FDCA. It must be said that this molecule, which is normally found in very low amount in the presence of base, due to its fast transformation to FDCA, was present with high quantity with respect to HMFCA.

Finally, the diacid product started to be formed at 30 minutes and its selectivity continued to increase throughout the reaction.

In order to verify the possibility to increase the catalytic activity by addition of a base, HMF oxidation was evaluated by adding 2 equivalents of the NaOH in the reaction medium (TableS2). As already observed for Pd-nNiO, also in the case of Au-nNiO, the higher pH did not increase the rate of FDCA formation. Indeed, HMF conversion was promoted (68% vs 15% after 30 min of reaction) and the yield in HMFCA was higher (36% vs 7%) but HMF degradation was predominant and carbon loss was found to be very high.

The significant change in the activity of Au-nNiO sample after few minutes of reaction in base-free conditions can be due to possible modification occurring to the catalyst and/or the inhibition effect on sample due to reactive intermediates produced during HMF oxidation. We can exclude the first hypothesis as TEM and XPS performed on Au-nNiO after 15, 30 min and 6 h of reaction did not show evident modifications in Au particle size and in Au oxidation state (Table 1).

For better understanding the specific role that the single reaction steps have on the overall reaction network, evaluation of the intermediates as starting reagents has been carried out using Au-nNiO (Table 2).

Table 2 Catalytic tests using reaction intermediates (FFCA, DFF and HMFCA) as starting material. Reaction conditions: 90°C, 2h, 10 bar O_2, HMF/total metal molar ratio = 100.

Entry	Reactant	Conv. (%)	FFCA sel (%)	FDCA sel (%)	Unkn X	Unkn. Y
1	FFCA	30	-	100	No	No
2	DFF	28	32	-	Yes	No
3	DFF[a]	17	27	-	Yes	No
4	DFF[b]	34	4	-	Traces	Yes
5	HMFCA	36	69	31	Traces	No

[a]Catalyst: used Au-nNiO; [b]Catalyst: nNiO

First, a preliminary experiment was carried out by reacting FFCA with the chosen catalyst, to verify its ability to convert this reaction intermediate. After 2 h of reaction, 30% conversion of FFCA was shown (Table 2, entry 1) with complete transformation of the reagent into FDCA, confirming the activity of the catalyst towards FFCA conversion with low conversion but high selectivity (100%).

The use of DFF as reactant with Au-nNiO catalyst (Table 2, entry 2) led to 28% conversion with formation of FFCA; however, when DFF was loaded with a catalyst already used for 30 minutes in HMF oxidation (Table 2, entry 3) a decrease in conversion was observed. This phenomenon could be ascribed to a partial covering of Au nanoparticles by NiO or to the catalyst activity inhibition in some of the oxidation steps.

Thus, in order to verify the first hypothesis, a test using bare nNiO to oxidise DFF has been carried out (Table 2, entry 4). In these experimental conditions, high DFF conversion was obtained (34%) but low FFCA selectivity was observed. It is evident that nNiO was inactive in HMF oxidation and promoted mainly the conversion of DFF. However, the formation of an undetected product (named as Y) was detected from HPLC analysis, meaning that bare nNiO reactivity significantly differs from the one showed by Au-nNiO; thus, the hypothesis of complete coverage of Au by nNiO cannot be corroborated since, using the metal supported catalyst, this unknown product was not formed. It is very important to underline that the product formed with nNiO was different from the one revealed in the other reactions when DFF was used. Moreover, it is worth to notice that FDCA is never formed when DFF is used as starting material, indicating that the only available route for its formation proceeds through HMFCA reaction pathway. Thus, it is possible to conclude that catalyst is probably inhibited by the presence of DFF, which prevents FFCA transformation to FDCA. The presence of DFF as reagent led also to the formation of an unknown compound, probably deriving from the furan ring opening. Therefore, a poisoning effect of DFF can be postulated, being FFCA conversion into FDCA hampered when DFF is fed. This suggestion has been confirmed by two further tests, where DFF and FFCA were used as starting material in different ratio. FDCA yield at the end of the 2h of reaction was around 2%, irrespective of the DFF/FFCA molar ratio (table S3). The obtained results are definitively far from that reported in Table 2 (entry 1) where higher amount of FDCA were formed, demonstrating the negative effect played by the presence of DFF in the diacid production.

The oxidation reaction using HMFCA as reagent (Table 2, entry 5) produced both FFCA and FDCA, confirming the possibility to produce the diacid through HMFCA reaction pathway.

AuPd-nNiO

AuPd-nNiO catalysts with nominal Au:Pd molar ratio of 6/4 were evaluated for HMF free-oxidation in terms of activity and long term stability. AuPd-nNiO catalyst displayed higher activity and selectivity to the desired product and a distinct catalytic behaviour compared to the monometallic Au-nNiO system as it is presented in Figure 5. Indeed, appreciable quantity of FDCA was already present at t=0, together with all the other reaction intermediates, i.e. DFF, HMFCA and FFCA. The shape of the curves representing FDCA and FFCA clearly shows the typical trend of consecutive products, while the amounts of detectable DFF and HMFCA were very low after the early period of the reaction. These two intermediates were both formed from HMF over AuPd-nNiO catalyst and their concentration decreased as a function of reaction time with a similar trend, despite of what observed for Au supported catalyst.

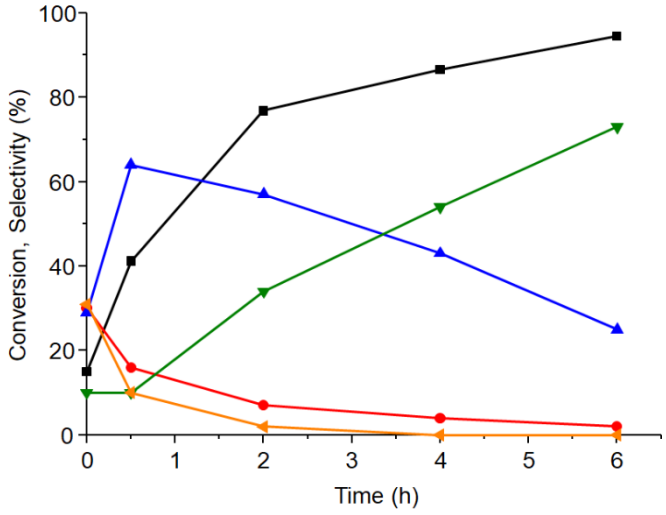

Figure 5 HMF Conversion and product selectivity as a function of time using AuPd-nNiO. Reaction conditions: 90 °C, 10 bar O_2, HMF/total metal molar ratio = 100. Legend: ■ HMF conversion, ● HMFCA selectivity, ◀ DFF selectivity, ▲ FFCA selectivity, ▶ FDCA selectivity.

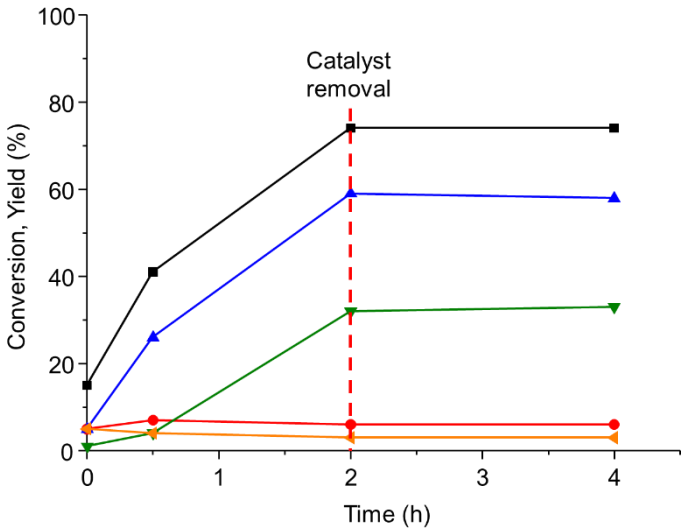

Figure 6 Leaching tests for the prepared AuPd-nNiO. Reaction conditions: 90 °C, 10 bar O_2, HMF/total metal molar ratio = 100. Legend: ■ HMF conversion, ● HMFCA selectivity, ◀ DFF selectivity, ▲ FFCA selectivity, ▶ FDCA selectivity.

In order to verify the ability of the bimetallic catalyst to convert these two different intermediates, HMFCA and DFF were separately used as reagent, (Table 3). After 2 h of reaction, high conversion of both molecules was obtained, demonstrating that FFCA can be produced efficient either from DFF or HMFCA. Although, the use of gold promoted FFCA formation from DFF, FDCA was not formed with this catalyst; on the contrary, the use of a bimetallic system favoured also FDCA formation from DFF. However, in terms of product selectivity a significant difference was observed, on the basis of the choice of reactant suggesting the presence, in the case of DFF of some inhibition effects on the transformation of FFCA to FDCA.

Table 3 Catalytic tests using reaction intermediates DFF and HMFCA as starting material. Reaction conditions: 90 °C, 2h, 10 bar O_2, Catalyst AuPd-nNiO, HMF/total metal molar ratio = 100.

Entry	Reactant	Conv. (%)	FFCA sel (%)	FDCA sel (%)
1	HMFCA	94	41	59
2	DFF	93	83	17

To verify the possibility of metal leaching and the participation of leached metal species in the reaction, a "hot filtration" catalytic test was performed in order to evaluate the activity of eventual leached metal species from the catalyst. This test was carried out by removing the catalyst after 2h of reaction and the resulting solution has been loaded in the autoclave immediately and charged with 10 bar of O_2 and kept at 90 °C for 2h (Figure 6). Since the conversion and the yields of the products remained unchanged it was excluded the effect of homogeneous metal species in the catalytic activity. To further exclude the leaching of metals from catalyst, XRF test was carried out on the filtered reaction solution after reactivity tests. Such tests revealed that no homogeneous metals species were found, thus metal leaching was excluded.

Since catalyst stability is one of the most important features that has to be taken into account during the development of a new material, reusability tests were carried out on the sample that showed the highest performance, i.e. the bimetallic AuPd system.

The reusability tests as shown in Figure 7 for the bimetallic catalyst showed a high level of stability after three times without any loss of activity; nevertheless, the fourth reaction carried out on the same material was accompanied by a small decrease in the catalytic performance. In fact, HMF conversion was steady for the first three uses (95%), after that this value dropped to 87%. Similarly, FDCA yield decreased from 70% of the first three uses to 55%. Characterisation of the used catalyst by means of TEM analysis was carried out and it was found that the average AuPd particle size of the used AuPd-nNiO catalyst was similar to the fresh (3.3 and 3.6 nm, for fresh and used AuPd-nNiO respectively, Table 1), even the formation of few aggregates was observed (Figure S6). However, XPS showed Au

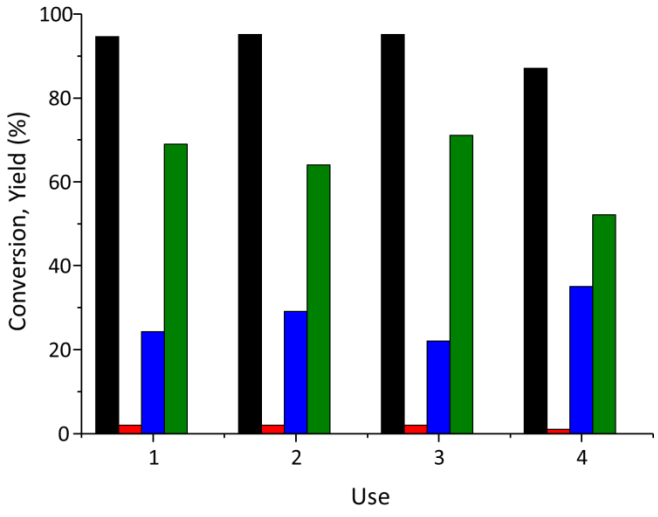

Figure 7 Reusability tests for the oxidation of HMF using AuPd-nNiO catalyst. Reaction conditions: 90 °C, 6h, 10 bar O_2, (HMF/total metal molar ratio = 100). Legend: ■ HMF conversion, ■ HMFCA yield, ■ FFCA yield, ■ FDCA yield, ■ DFF yield.

4f and Pd 3d peaks with a reduced intensity (Figure S7), probably due to the adsorption of the products on the active sites.

Conclusions

In summary, we have developed effective, stable NiO-based supported Au-Pd catalysts that can efficiently promote the base-free oxidation of HMF to FDCA in water using molecular oxygen at mild reaction conditions. By using a specific Au:Pd metal composition (6/4 atomic ratio) depositing preformed Au/Pd nanoparticles on nNiO as the chosen support, we succeeded to improve not only catalytic activity but also to enhance the yield to FDCA, by minimising the synthesis of side by-products and to improve overall the catalyst stability. NiO acts as an effective support providing basic sites that can promote the reaction and the proper choice of Au-Pd chemical composition favours the formation of FDCA. Moreover, by performing the aerobic oxidations of intermediates, like, DFF, FFCA, HMFCA in the presence of bare NiO, Au-nNiO and AuPd-nNiO, we found that the presence of nNiO promoted mainly the conversion of DFF to FFCA (scheme 1, pathway a) and only with the addition of Au the activation of HMF was favoured, showing the synergistic effect between Au and nNiO. Moreover, in the presence of Au formation of the consecutive products HMFCA, FFCA and FDCA were observed. Addition of a second metal like Pd with Au/Pd atomic ratio of 6/4 promoted significantly the rate of HMF formation and the yield to FDCA (69%). By studying the catalytic performance of HMFCA and DFF intermediates it was evident that both reaction pathways were observed with high activity and the addition of Pd further enhanced the oxidation of FFCA to FDCA, a difficult elementary reaction step in the presence of supported monometallic Au catalysts under base-free conditions. Finally, we present an effective catalytic system that can promote the oxidation of HMF to FDCA with high yield, activity and good level of stability without the use of base, making the process more green and cost-effective.

Conflicts of interest

There are no conflicts to declare

Acknowledgements

This work was co-funded through a SINCHEM Grant. SINCHEM is a Joint Doctorate program selected under the Erasmus Mundus Action 1 Programme (FPA 2013-0037).

References

1. R. A. Sheldon, *Green Chemistry*, 2014, **16**, 950-963.
2. J. J. Bozell and G. R. Petersen, *Green Chemistry*, 2010, **12**, 539-554.
3. R.-J. van Putten, J. C. van der Waal, E. de Jong, C. B. Rasrendra, H. J. Heeres and J. G. de Vries, *Chemical Reviews*, 2013, **113**, 1499-1597.
4. A. A. Rosatella, S. P. Simeonov, R. F. M. Frade and C. A. M. Afonso, *Green Chemistry*, 2011, **13**, 754-793.
5. A. Gandini, A. J. D. Silvestre, C. P. Neto, A. F. Sousa and M. Gomes, *Journal of Polymer Science Part A: Polymer Chemistry*, 2009, **47**, 295-298.
6. H. Nakajima, P. Dijkstra and K. Loos, *Polymers*, 2017, **9**, 523.
7. https://www.mordorintelligence.com/industry-reports/global-polyethylene-teraphtalate-market-industry, (accessed March 15th, 2018).
8. Z. Zhang and K. Deng, *ACS Catalysis*, 2015, **5**, 6529-6544.
9. US20150051412.
10. W. Partenheimer and Vladimir V. Grushin, *Advanced Synthesis & Catalysis*, 2001, **343**, 102-111.
11. H. Ait Rass, N. Essayem and M. Besson, *ChemSusChem*, 2015, **8**, 1206-1217.
12. O. Casanova, S. Iborra and A. Corma, *ChemSusChem*, 2009, **2**, 1138-1144.
13. Y. Y. Gorbanev, S. K. Klitgaard, J. M. Woodley, C. H. Christensen and A. Riisager, *ChemSusChem*, 2009, **2**, 672-675.
14. Z. Miao, Y. Zhang, X. Pan, T. Wu, B. Zhang, J. Li, T. Yi, Z. Zhang and X. Yang, *Catalysis Science & Technology*, 2015, **5**, 1314-1322.
15. J. Cai, H. Ma, J. Zhang, Q. Song, Z. Du, Y. Huang and J. Xu, *Chemistry – A European Journal*, 2013, **19**, 14215-14223.
16. K. R. Vuyyuru and P. Strasser, *Catalysis Today*, 2012, **195**, 144-154.
17. S. E. Davis, B. N. Zope and R. J. Davis, *Green Chemistry*, 2012, **14**, 143-147.
18. S. Albonetti, T. Pasini, A. Lolli, M. Blosi, M. Piccinini, N. Dimitratos, J. A. Lopez-Sanchez, D. J. Morgan, A. F. Carley, G. J. Hutchings and F. Cavani, *Catalysis Today*, 2012, **195**, 120-126.
19. A. Lolli, S. Albonetti, L. Utili, R. Amadori, F. Ospitali, C. Lucarelli and F. Cavani, *Applied Catalysis A: General*, 2015, **504**, 408-419.
20. X. Wan, C. Zhou, J. Chen, W. Deng, Q. Zhang, Y. Yang and Y. Wang, *ACS Catalysis*, 2014, **4**, 2175-2185.
21. C. Zhou, W. Deng, X. Wan, Q. Zhang, Y. Yang and Y. Wang, *ChemCatChem*, 2015, **7**, 2853-2863.
22. N. K. Gupta, S. Nishimura, A. Takagaki and K. Ebitani, *Green Chemistry*, 2011, **13**, 824-827.
23. Z. Gao, R. Xie, G. Fan, L. Yang and F. Li, *ACS Sustainable Chemistry & Engineering*, 2017, **5**, 5852-5861.
24. J. Artz and R. Palkovits, *ChemSusChem*, 2015, **8**, 3832-3838.
25. G. Yi, S. P. Teong and Y. Zhang, *Green Chemistry*, 2016, **18**, 979-983.
26. D. K. Mishra, H. J. Lee, J. Kim, H.-S. Lee, J. K. Cho, Y.-W. Suh, Y. Yi and Y. J. Kim, *Green Chemistry*, 2017, **19**, 1619-1623.
27. D. Yan, J. Xin, C. Shi, X. Lu, L. Ni, G. Wang and S. Zhang, *Chemical Engineering Journal*, 2017, **323**, 473-482.
28. A. Villa, C. E. Chan-Thaw, G. M. Veith, K. L. More, D. Ferri and L. Prati, *ChemCatChem*, 2011, **3**, 1612-1618.
29. L. Prati, A. Villa, F. Porta, D. Wang and D. Su, *Catalysis Today*, 2007, **122**, 386-390.
30. A. Villa, G. M. Veith, D. Ferri, A. Weidenkaff, K. A. Perry, S. Campisi and L. Prati, *Catalysis Science & Technology*, 2013, **3**, 394-399.
31. G. M. Veith, A. R. Lupini and N. J. Dudney, *The Journal of Physical Chemistry C*, 2009, **113**, 269-280.

32. A. Villa, N. Dimitratos, C. E. Chan-Thaw, C. Hammond, G. M. Veith, D. Wang, M. Manzoli, L. Prati and G. J. Hutchings, *Chemical Society Reviews*, 2016, **45**, 4953-4994.
33. C. E. Chan-Thaw, A. Villa, G. M. Veith and L. Prati, *ChemCatChem*, 2015, **7**, 1338-1346.
34. E. H. Voogt, A. J. M. Mens, O. L. J. Gijzeman and J. W. Geus, *Surface Science*, 1997, **373**, 210-220.
35. C. E. Chan-Thaw, A. Villa, D. Wang, V. D. Santo, A. Orbelli Biroli, G. M. Veith, A. Thomas and L. Prati, *ChemCatChem*, 2015, **7**, 2149-2154.
36. J. Radnik, C. Mohr and P. Claus, *Physical Chemistry Chemical Physics*, 2003, **5**, 172-177.
37. M. P. Casaletto, A. Longo, A. Martorana, A. Prestianni and A. M. Venezia, *Surface and Interface Analysis*, 2006, **38**, 215-218.
38. A. Villa, A. Gaiassi, I. Rossetti, C. L. Bianchi, K. van Benthem, G. M. Veith and L. Prati, *Journal of Catalysis*, 2010, **275**, 108-116.
39. H.-Y. Park, T.-Y. Jeon, J. H. Jang, S. J. Yoo, K.-H. Choi, N. Jung, Y.-H. Chung, M. Ahn, Y.-H. Cho, K.-S. Lee and Y.-E. Sung, *Applied Catalysis B: Environmental*, 2013, **129**, 375-381.
40. A. Villa, A. Jouve, F. J. Sanchez Trujillo, D. Motta, L. Prati and N. Dimitratos, *Catalysts*, 2018, **8**, 54.
41. A. Villa, M. Schiavoni, S. Campisi, G. M. Veith and L. Prati, *ChemSusChem*, 2013, **6**, 609-612.
42. T. Pasini, M. Piccinini, M. Blosi, R. Bonelli, S. Albonetti, N. Dimitratos, J. A. Lopez-Sanchez, M. Sankar, Q. He, C. J. Kiely, G. J. Hutchings and F. Cavani, *Green Chemistry*, 2011, **13**, 2091-2099.